Functionalization of open-celled foams by homogeneous slurry based coatings

Daniela Boettge,[a] Gisela Standke, Alexander Fuessel, and Jörg Adler
Nonoxide Ceramics, Fraunhofer Institute for Ceramic Technologies and Systems IKTS Dresden, Winterbergstrasse 28, D-01277 Dresden, Germany

(Received 11 February 2013; accepted 18 April 2013)

A new technology to coat open-celled foams homogeneously by using a vertical centrifuge and shear-thinning slurries is presented. The technology is exemplified by a complex multilayer-coated foam for catalytic applications (Fig. 3). Furthermore, a new calculation model for the estimation of coating thickness and for quality assessment is introduced and proved by comparing the calculated and experimental data. Based on these results, various material combinations are shown, e.g., layers made of rough particles, zeolites, activated carbon, γ-Al_2O_3, perovskites, mullite, and yttria–alumina–garnet on SiC–, Al_2O_3–, or cordierite foams. Theses "functionalized foams" can be used for a wide variety of practical applications, e.g., as adsorbents and catalysts in environmental engineering, as preforms for metal matrix composites, and for special purpose applications that require corrosion and oxidation resistance.

I. INTRODUCTION

Components made of porous ceramics or metals are well-established in the field of environmental technology, such as filtration processes at high temperatures, modern burner technologies, or solar power plants.[1] For this reason, large quantities of several hundreds of millions of replica foams made by Schwartzwalder technology[2] are produced per year all over the world.

Nowadays, new challenges in process engineering and environmental technologies not only require cellular materials that offer functional properties like corrosion resistance, catalytic activity, or adhesion characteristics. They also require outstanding structural properties including high open porosity and network-like structures. One option to open up these new areas of application is the functionalization of ceramic foams by surface coating.

In the context of catalysis, several sources refer to coatings on open-celled ceramic foams.[3–5] Yet often the used coating methods are not described in detail. Moreover, most of these techniques are derived from coating dense elements and are therefore not really suitable for foam structures with their high storage properties for liquids. This results in the production of only thin and inhomogeneous coatings. However, this outcome could be improved by repeating several dip coating steps. The disadvantage of this procedure is its low efficiency. Thus, it is important to improve these coating techniques to create new strategies for functionalizing sintered foam materials. This includes surface characteristics of the foam structure as well as rheological properties of the coating slurries and the coating technology itself.

This work aims to present solutions for the above-mentioned issues and shows the possibility of coating foam surfaces with homogeneous functional layers. The used techniques allow to build up various interesting material combinations of "foam + functional layer" that can be adapted to a wide variety of applications. Furthermore, a new calculation model for coating thickness estimations is also presented and compared with experimental derived coatings on foams. Finally, some practical applications for these coatings are described, e.g., functional coatings for purposes of catalytic coatings, corrosion resistance, and preforms for metal matrix composites (MMCs).

II. CERAMIC AND METAL FOAMS

The main production technique of open-celled foams is the replication technique introduced by Schwartzwalder and Somers.[2] In this method, polyurethane templates are coated with aqueous shear-thinning slurries. The slurries usually consist of ceramic or metallic powder, dispersing agents, and auxiliaries for binding as well as rheological additives. The coating procedure is divided into an impregnation and a homogenization step. During impregnation, the foam templates were squeezed to make sure the slurry covers all polymeric struts. Roller machines are commonly used to homogenize the slurry coating. However, centrifugation is a better alternative since it produces very homogeneous coatings over the entire component of the

[a]Address all correspondence to this author.
e-mail: daniela.boettge@ikts.fraunhofer.de
DOI: 10.1557/jmr.2013.127

 © Materials Research Society 2013

https://doi.org/10.1557/jmr.2013.127 Published online by Cambridge University Press

polymeric foam without the accumulation of material at the edges. This is especially important in applications where homogenous material distribution is highly preferred, e.g., burner or catalytic applications. After the impregnation and homogenization treatment of the polymeric foams with the slurry, they subsequently pass through heat treatment steps, i.e., drying, pyrolysis, and sintering.

Ceramic foams made of silicate-bonded silicon carbide, alumina, and zirconia (ZrO_2) are commonly used in the industry. Currently, molten metal filtration is the main field of application of ceramic foams.[6–11] Due to their open-celled structure, ceramic foams have attracted great interest in other fields of application. In the past few decades, a lot of researchers have been trying to create new materials with higher chemical purity and enhanced properties compared with the conventional quality of metal filters.[12,13] Two examples worth mentioning are LigaFill®-foams made of siliconized silicon carbide with nearly dense ceramic struts[14,15] and an extremely higher strength than conventional foam materials (Fig. 1) as well as pure sintered silicon carbide (SSiC) foams with one of the highest thermal stabilities among the suitable materials for burners.[16]

There are different approaches to manufacture materials and components made of open-celled metal foams including investment casting, chemical vapor deposition coating,[17] galvanic deposition, and powder-based replication[18] and their combinations. However, the practical application of these methods is limited on a few fields such as bone replacement[19,20] and automotive retrofit catalyst carriers.[21,22] Nevertheless, a large variety of materials ranging from nonferrous metals to different steel alloys can be manufactured as open-celled foams by the replication method (Table I).

An important issue for the use of ceramic or metal foams is the characterization of their cellular structure as well as their resulting cell size after coating with functional layers. Their structure is commonly described as being a set of distorted pentagon-dodecahedrons or tetrakaidecahedrons or combinations of both.[32] This cell structure is determined by the reticulated polyurethane foams used. These are usually classified by their mean cell sizes measured in pores per inch (ppi) according to an American Society for Testing and Materials standard[33] in a range of 8–90 ppi. This standard does not illustrate the foam structure sufficiently since there is a big difference between the cell (the former bubble diameter) and the cell windows. Neither these different cell sizes nor their distortions are registered by the measurement with the above-mentioned standard. For this reason, new characterization methods using computer tomography or special cell-counting techniques are under development. But at present, no commercially used methods exist. One alternative is a special optical method where only the surface of the foams is lighted.[34] As a result, only the struts on the surface are pictured making it possible to reconstruct the foam cells. The equivalent circular diameter (ecd) of these reconstructed cells acts as a measurement value and provides more information about the material used and their prospective properties. The measurement technique works very fast compared with computer tomography. Moreover, it can both be used for controlling the quality of polyurethane foams as well as sintered structures.

Another important characteristic of foam structures, especially in the context of functional coatings, is the specific geometrical surface area S_{geo}, which specifies the surface that is available for the coating material per volume. Until now, there has been a lack of suitable measurement methods for the experimental determination of this important parameter.

However, academic literature offers several model calculations on the estimation of the specific geometrical surface. The basis for more complex models was presented by Gibson and Ashby[35] who illustrated the foam cell as a specific regular network, such as a package of cubic cells, hexagonal prisms, rhombic dodecahedrons, or tetrakaidecahedrons. Based on this work, further models were developed, e.g., by Richardson et al.[36] and Buciuman and Kraushaar-Czarnetzki.[37] A similar approach was chosen by Grosse et al.[38] Her calculation model is based on the Weaire–Phelan structure and shows a good correlation to data determined by magnetic resonance tomography (MRT) of alumina and silicon carbide foams. According to this model, the specific geometrical surface area S_{geo} depends on the diameter of the cell window d_w, the diameter of the foam strut d_s, and the open foam porosity ε_0 [Eq. (1)].

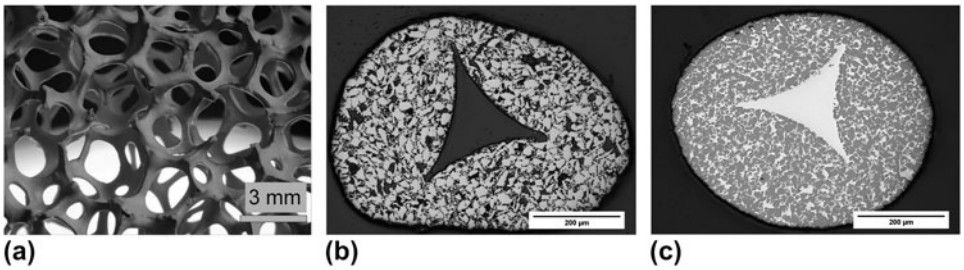


FIG. 1. (a) Typical foam structure, (b) hollow and microporous SSiC-foam strut, and (c) dense SiSiC-foam strut (LigaFill®).

https://doi.org/10.1557/jmr.2013.127 Published online by Cambridge University Press

TABLE I. Sintered replica foams and their main properties.

Material	Properties or selection criteria
Ceramics	
Silicon carbide (sintered, SSiC)[23,24]	Thermal resistance up to 1500 °C, high thermo-shock stability
Silicon carbide (siliconized, SiSiC)[15,25,26]	Five times higher strength compared with common ceramics
Silicon carbide (clay-bonded SiC)	Most cost-effective silicon carbide
Alumina (Al_2O_3)	Low thermal conductivity, electrical insulation
Cordierite	Low thermal expansion, cost effective
Metals	
Alloyed steel, e.g., FeCrAl[27]	High thermal stability up to 1100 °C, ductile
Stainless steel[28]	High corrosion resistance, ductility, biocompatibility
Titanium[29], molybdenum[30,31], tantalum	Special applications for thermal insulation, bone substitution, lightweight constructions

$$S_{\mathrm{geo}} = \frac{4.84(1-\varepsilon_0)^{0.5} - 2.64(1-\varepsilon_0)}{d_{\mathrm{F}} + d_{\mathrm{s}}} \quad . \qquad (1)$$

Another model that focuses on metallic foams was derived by Giani et al.[39] A paper by Inayat et al.[40] provides a good overview on the different models for simulation of foam structure known from the literature. The calculation of this model takes the shape of the foam struts that depend on the open foam porosity ε_0 into consideration.

III. COATING OF FOAM STRUCTURES

A. State of the art

Currently, catalytic coating is the most frequently used method for the functionalization of open-celled foams. However, apart from research and development, there has not been any significant industrial application yet. Catalytic coating of open foams has been used in scientific research for catalysis processes that include oxidation of hydrogen,[41,42] oxidation of carbon monoxide (CO),[43] combustion of hydrocarbons, e.g., methane,[44,45] partial oxidation of methanol,[46] and in classical catalytic processes, such as water gas shift reaction and Fischer–Tropsch synthesis.[47,48] A paper by Reitzmann et al.[49] provides a good overview on previous publications on catalytic coatings of foams and also summarizes the extensive work of Twigg and Richardson.[50–52]

Although many papers about research activities done on open-celled foams as catalyst supports can be found, information on the coating technology itself is very limited. This problem is especially highlighted by the lack of description of materials and process technologies applied. Most described coating methods are slurry-based. In this method, cellular structures are dipped into slurry or a precursor solution of the catalytically active material,[3–5,53] and the excessive slurry is removed by shaking or blowing with compressed air.[51,54] The used slurries or precursor solutions often have a very low viscosity to prevent them from blocking the network-like structure of the foam. This approach leads to thin and irregular layers on the foam struts. After drying and calcination, the same coating method is repeated until the desired loading is reached.[52,55]

In summary, the literature available shows that a homogeneous and entire coating of the three-dimensional network is a key task for the implementation of foams into a wide range of industrial applications. Compared with plane substrates, foams possess a high surface area-to-volume ratio, which leads to additional effects (e.g., capillarity) that must be taken into account using slurry-based coating methods. To meet the challenge of homogeneous coating, the rheology of slurries needs to be adjusted according to the coating technology. This concerns both the characteristics like wetting of the whole foam network and adhesion on the foam struts.[49] To improve adhesion, scientific papers mention different ideas for the pretreatment of foam surfaces, e.g., the oxidation of silicon carbide foams or etching in case of metallic foams.[4]

B. New coating technology

The coating technology described in this paper is a combination of dip coating and spin coating using a vertical centrifuge (diameter: 1100 mm, maximum rotational speed: 1000 1/min, spin efficiency "*C*" max: 615). During the first step ("dip coating") where the foam is dipped into the coating slurry, special care must be taken to ensure that the network is completely saturated and wetted with slurry. This procedure depends on the foam size but it is usually completed after a short immersion time of about 10 s. After dipping, the ceramic foam is removed from slurry and drained to have a minimal loss of the same.

In the second step ("spin coating"), a vertical centrifuge is used to remove excessive slurry from the foam network (Fig. 2). A homogeneous layer of a defined thickness is formed depending on the chosen process parameters (particularly speed of rotation) and slurry properties [e.g., solid content (sc)]. The coating quality is considered perfect when the foam network is both completely coated and open-celled at the same time. Otherwise, the core of especially large foam components could be blocked and might cause undesirable effects in its practical application (e.g., a high pressure drop or inhomogeneous gas flow in chemical reactors).

The size of the foams that can be coated by the above-described method is limited by the size of the centrifuge basket. Inserts with a dimension of 500 × 500 mm

https://doi.org/10.1557/jmr.2013.127 Published online by Cambridge University Press

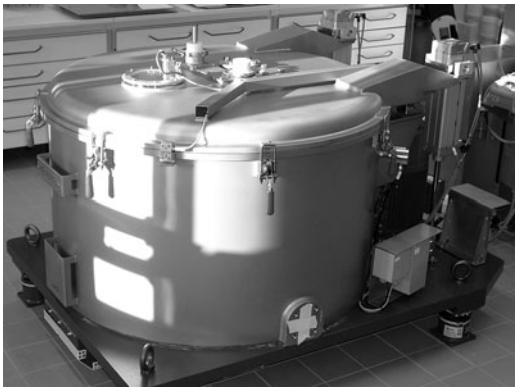


FIG. 2. Vertical centrifuge used for coating open-celled foams.

were used for this work. Consequently, it is possible to upscale this coating technology to large-sized foam structures, which can have various interesting industrial applications.

The coating technology enables the deposition of functional layers of a definite thickness of up to 100 μm. Therefore, it is necessary to develop coating slurries of an adapted flow behavior and comparably high sc—in contrast to conventional washcoat techniques which often use low-concentrated precursor solutions with Newtonian flow behavior. The slurry viscosity must be low enough to immerse the whole network during dipping or centrifugation. However, the slurry also needs to have a high enough viscosity to ensure a good adhesion on the foams struts and to form homogeneous functional layers of a certain thickness. To adjust this flow behavior, special binder systems and additives are used to meet these required processing characteristics.

C. Calculation model for the estimation of coating thickness

For the practical application of the coating technology, it might be beneficial to first identify the optimum process parameters (e.g., sc of the slurry or rotational speed of the centrifuge) to reach high-quality coatings of targeted layer thicknesses. Based on the technological parameters of the developed coating technology and the shear-thinning flow behavior of the slurries, a new calculation model for estimation of coating thickness on the foam struts was derived. This calculation model differs entirely from existing models of Landau and Levich[56] describing the flow of Newtonian liquids during the dip coating process or Emslie et al.[57] describing the flow of Newtonian liquids during the spin-coating process.

Similar to the developed coating technology, the new calculation model includes both the process steps of dipping and centrifugation. During the first step, the layer thickness d_{dip} that is formed by dipping can be calculated as a result of the weight force of the slurry layer [Eq. (2)]. The main influence parameters on this maximum attainable layer thickness are the yield point τ_0 and the slurry density ρ_S.

$$d_{dip} = \frac{\tau_0}{\rho_S \cdot g} \quad . \tag{2}$$

The layer thickness d_{dip} is an important parameter for the determination of the layer thickness d_{spin}, which is formed by centrifugation (spinning) as a result of the centrifugal force. For the estimation of the layer thickness d_{spin}, a new process-related slurry parameter called, the "representative shear stress," τ_{rep} is defined. The experimental determination of this parameter is discussed below. The layer thickness d_{spin} also depends on the slurry density ρ_S and on the technological parameter radial acceleration a_r [Eq. (3)].

$$d_{spin} = \frac{\tau_{rep}}{\rho_S \cdot a_r} \quad . \tag{3}$$

The radial acceleration a_r can be regulated by the rotational speed N of the centrifuge and depends on the distance between the centrifuge insert and the center of the centrifuge R where the foam sample is located [Eq. (4)].

$$a_{r(R)} = \frac{v^2}{R} = 4\pi^2 RN^2 \text{ with } v = 2\pi RN \quad . \tag{4}$$

This shows that to calculate the medium layer thickness $\bar{d}_{spin}$ of a foam sample with the thickness D, the distance between the centrifuge insert and the center of the centrifuge reduced by the half foam thickness $D/2$ must be taken into account [Eq. (5)].

$$\bar{d}_{spin} = \frac{\tau_{rep}}{\rho_S \cdot a_r (R - D/2)} \quad . \tag{5}$$

In this way, it is possible to calculate the layer thickness of the foam sample at every point. The gradient of layer thickness along the sample thickness $\frac{\Delta d_{spin}}{D}$ can be calculated using Eq. (6).

$$\frac{\Delta d_{spin}}{D} = \frac{d_{spin(R-D)} - d_{spin(R)}}{D} = \frac{\frac{\tau_{rep}}{4\pi^2 \cdot N^2} \cdot \left(\frac{1}{R-D} - \frac{1}{R}\right)}{D} \quad . \tag{6}$$

One general remark is that the results of Eqs. (2) and (3) are the thicknesses of the wet layers. To calculate the layer thickness after heat treatment, i.e., drying or sintering, both equations need to be multiplied by the appropriate value of the layer shrinkage.

Giving the fact that d_{spin} could never reach a higher value than d_{dip} the "minimal radial acceleration" a_{r_min} is defined first. This parameter is obtained from the ratio of τ_{rep} to τ_0 [Eq. (7)] and must be set as the minimum value at the centrifuge to remove slurry from the saturated foam

https://doi.org/10.1557/jmr.2013.127 Published online by Cambridge University Press

network and, thus, to ensure homogenous and particularly open-celled coatings.

$$a_{r_min} > \frac{\tau_{rep} \cdot g}{\tau_0} \quad . \tag{7}$$

In conclusion, the calculation with the parameters τ_0, τ_{rep}, a_r, or N enable both the quantitative estimation of the layer thickness and the qualitative prediction of the coating result. For the application of the model, all the mentioned parameters need to be determined experimentally. In this case, the yield point τ_0 and the representative shear stress are the results of rheological measurement using oscillating and rotating methods. The yield point is determined by means of the oscillatory tests "amplitude sweep," as the value of shear stress τ that corresponds to the intersection of the curves for storage modulus G' and loss modulus G''.[58]

The representative shear stress τ_{rep} is identified by rheological rotation tests where the viscosity is measured as a function of the applied shear stress [Eq. (8)].

$$\eta = f(\tau) \quad . \tag{8}$$

This function enables the determination of τ_{rep} as the point where the viscosity of the shear thinning slurry shows nearly no decrease anymore. Mathematically, τ_{rep} can be expressed as the value of shear stress where the slope of the curve approaches zero. In this work, τ_{rep} was determined when the slope m of the curve reached 0.1 Pa/mPa s:

$$m = f'(\tau_{rep}) = 0.1 \frac{\text{Pa}}{\text{mPa s}} \quad . \tag{9}$$

Besides the evaluation of τ_0 and τ_{rep} by rheological measurements, the slurry density was determined by the liter weight method. The radial acceleration a_r as procedural variable can be adjusted by the rotational speed N of the centrifuge.

D. Example of proof: Comparison of experimental and calculated data

The correlations described above have been verified by a number of experiments. In this section, the validity of both the coating technology and the calculation model is presented by the example of one specific washcoat for catalytic applications.

Due to foam supports having special advantages in the field of catalytic high temperature applications like highly exothermic oxidation reactions, a multilayer washcoat system with a thermal resistance of up to 1300 °C is used to illustrate the comparison of experimental and calculated data. As depicted in Fig. 3, the material system consists of a thermal shock resistant SSiC foam as support, a layer with rough SiC particles, a mullite intermediate layer, and a calcium aluminate (CA) washcoat.[59] The illustrated multilayer system exemplifies the different effects of the functional layers. The task of the first layer that consists of rough SiC particles is to improve the adhesion and homogeneous dispersion of the next layers on the SSiC foam struts. The mullite intermediate layer is applied in between the SiC foam and the CA washcoat. The function of the mullite intermediate layer is to prevent reactions between SiO_2 (oxidized SiC) and CA at high operating temperatures and to guarantee the thermal stability of the material combinations of the "foam/washcoat." The CA washcoat determines the application characteristics of the multilayer system. It mainly consists of calcium hexaaluminate (CA_6) as the primary phase and provides a high specific surface area at temperatures of up to 1200 °C.

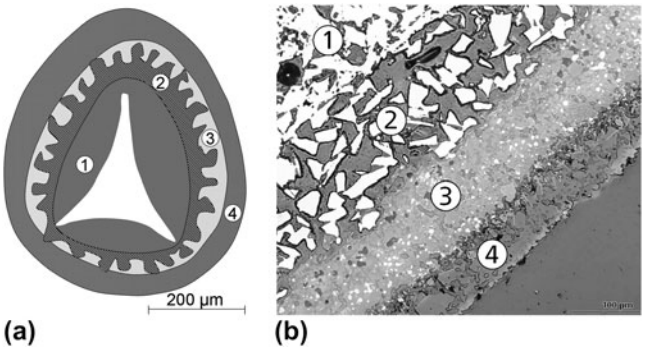


FIG. 3. Square section of the multilayer system for catalytic applications: (a) schematic figure and (b) light microscopic image (1, hollow SiC ceramic strut; 2, layer with rough SiC particles; 3, mullite intermediate layer; and 4, CA washcoat layer).

The applicability of the coating technology and the comparison between the experimental and calculated data are described by using the CA washcoat layer as an example. Systematic coating tests have been carried out on SSiC foam samples with a cubic dimension of 40 × 40 × 25 mm^3. CA slurries with three different sc (45wt%, 50 wt%, 54 wt%) were developed and characterized to determine the required material parameters for the calculation of the layer thicknesses d_{dip} and $\bar{d}_{spin}$ of the CA washcoat layers by using Eqs. (2) and (5). The composition of the CA slurries is shown in Table II. The coating layers consisting of the CA phase were formed in situ on the foam by calcination of the slurry layers at 1200 °C.

All the developed suspensions with three different sc were stable and they were not prone to sedimentation. They showed the desired shear thinning flow behavior and a yield point. Table III summarizes the results of slurry characterizations including the obtained drying and sinter shrinkage values (s_{total}) at 1200 °C.

As expected, the values of slurry density ρ_S, yield point τ_0, and representative shear stress τ_{rep} increase, whereas the drying and sinter shrinkage s_{total} of CA layers decreases with a higher level of slurry sc. In addition to this

https://doi.org/10.1557/jmr.2013.127 Published online by Cambridge University Press

TABLE II. Slurry composition used for the formation of the CA washcoat layers.

Composition	Product type	Amount of active ingredients (wt%)
Powder 1 (d_{50} = 0.9 μm)	$Al(OH)_3$	91.5
Powder 2 (d_{50} = 1.6 μm)	$CaCO_3$	8.5
Auxiliaries, calculated on the total amount of powder		
Dispersing agent	Synthetic polyelectrolyte	1.4
Binder	Polyvinyl alcohol	1.0
Rheological additive	Hydrocolloid	0.15
Purified water	→ Required amount for sc of 45, 50, and 54 wt%	

TABLE III. Material parameters of the developed CA slurries and CA layers (sc: solid content, ρ_S: slurry density, τ_0: yield point, τ_{rep}: representative shear stress, s_{total}: drying and sinter shrinkage of CA layers).

sc (wt%)	ρ_S (g/cm^3)	τ_0 (Pa)	$\tau_{rep.}$ (Pa)	s_{total} (%)
45	1.35	0.73	26	36.2
50	1.39	1.32	37	35.1
54	1.41	1.75	58	34.6

variation of the material parameters, the radial acceleration has been varied in three steps by regulating the rotational speed, N, of the centrifuge shown in Fig. 2. These three different rotational speeds and the corresponding radial accelerations in the middle of the foam samples are presented in Table IV.

Before the experimental determination of the CA washcoat layer thickness, the calculation model was applied first using material and technical parameters shown in Tables III and IV. At first, the required minimal radial acceleration a_{r_min} that should be assigned at the centrifuge to remove the slurry out of the saturated foam network was calculated by using Eq. (7). Table V shows the required values for a_{r_min} and the corresponding minimal rotational speeds N_{min}, which depend on the sc of the CA slurries.

The calculated results of N_{min} reveal that a rotational speed of 300 min^{-1} is insufficient to cause a decrease in the layer thickness compared with the dipping step of all three sc. This is confirmed by the experimental results as illustrated in Fig. 4 by stereomicroscopic images.

Figure 4(a) shows a good coating quality that was reached by the coating of SSiC foams (ppi20) with a CA slurry (sc: 54 wt%) at a rotational speed N of 500 min^{-1} that is higher than the calculated minimal rotational speed N_{min}. The stereomicroscopic image shows a complete open-celled foam network and homogeneously coated foam struts. Whereas Fig. 4(b) illustrates that a rotational speed of 300 min^{-1} was insufficient to remove the slurry that drains from the foam struts and accumulates in the foam

TABLE IV. Rotational speeds and corresponding radial accelerations, $a_{r(R\ -\ D/2)}$ in the middle of the foam samples.

N (min^{-1})	$a_{r(R)}$ (m/s^2)
300	207
400	368
500	576

TABLE V. Required minimal radial acceleration a_{r_min} and minimal rotational speeds N_{min} depending on the sc of the CA-slurries.

sc (wt%)	a_{r_min} (m/s^2)	N_{min} (min^{-1})
45	349	402
50	275	356
54	325	388

cells and thus blocking the cell structure. Thus, Fig. 4 demonstrates that a_{r_min} is generally a good parameter for assessing the coating quality.

Table VI shows the calculated thicknesses for sintered CA layers $d_{dip,si.}$ and $d_{spin,si.}$ in relation to sc and rotational speed N, which were calculated with Eqs. (2) and (5) using material and technical parameters mentioned previously in Tables III and IV. Compared with the previous results, it becomes apparent that the theoretical layer thicknesses $d_{spin,si.}$ for 300 min^{-1} are higher than the layer thicknesses $d_{dip,si.}$ This implies the necessity to adjust the rotational speed of the centrifuge.

After calculation the layer thickness was measured on at least three samples per parameter variation according to German Institute for Standardization (DIN EN 1071-10) using scanning electron microscopic (SEM) and light microscopic images. Special care was taken to measure only foam struts with nearly perpendicular cut. Figure 5 shows two examples in measuring the layer thickness of two different CA layers.

Table VII summarizes the mean values and standard deviations (±) of the measured thicknesses of sintered CA layers in dependence of the sc of the CA slurry and the rotational speed N of the centrifuge.

As shown in Fig. 6, the results show that the measured and calculated values match each other well.

Another quick method for estimating the layer thickness is the differential weighing of the foam samples both before and after layer deposition. By using Eq. (10), the resulting coating mass m_{dw} can be converted to a corresponding layer thickness d_{dw}. The equation assumes the layer thickness to be homogenously distributed at the entire substrate ($m_{foam+layer}$ = mass of the coated substrate, $m_{substrate}$ = mass of the uncoated substrate, S_{geo} = specific geometrical surface area of the foam, V_{foam} = volume of the foam sample, and ρ_{layer} = density of the coating).

https://doi.org/10.1557/jmr.2013.127 Published online by Cambridge University Press

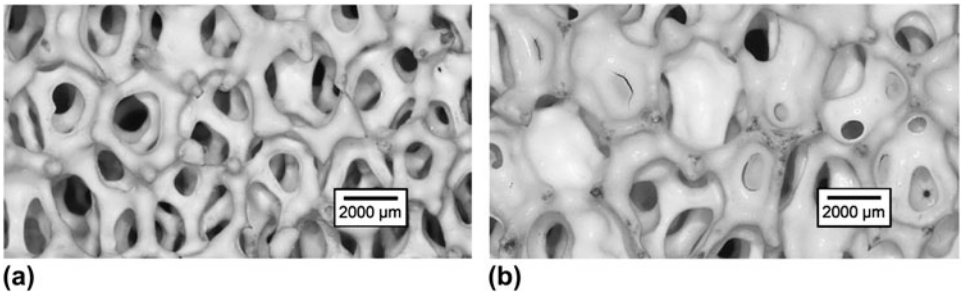


FIG. 4. Stereomicroscopic images of a CA-coated foam network with different chosen parameters (a) sc: 54 wt%; N: 500 min^{-1} and (b) sc: 54 wt%; N: 300 min^{-1}.

$$d_{\mathrm{dw}} = \frac{\left(m_{\mathrm{foam+layer}} - m_{\mathrm{foam}}\right)}{S_{\mathrm{geo}} V_{\mathrm{foam}} \rho_{\mathrm{layer}}} \quad . \qquad (10)$$

Figure 7 shows the measured masses of the sintered CA layers $m_{\mathrm{CA,si.}}$ depending on the sc and the rotational speed, N. The masses refer to foam samples having a cubic dimension of 40 × 40 × 25 mm^3 and a cell size of 20 ppi. As expected, the coating masses increase with decreasing rotational speed and increasing the sc. The amount of washcoat loading that can be achieved during coating of SSiC foams (20 ppi) by CA washcoat ranges from 15.5 to 60.8 g/L depending on the sc of the coating slurry and rotational speed, N, of the centrifuge.

Based on the results as summarized in Fig. 7, the layer thickness was calculated according to Eq. (10) by using the sample volume, V_{foam}, of 40,000 mm^3 (40 × 40 × 25 mm^3) and the specific geometrical surface area, S_{geo}, of about 920 m^2/m^3, which was calculated by Eq. (1). The results in Table VIII show a good level of congruency between the calculated and the measured values and thus verifying successful prediction of coating thickness by a simple weighing method.

In summary, it is proved that the new coating technology can be described by the calculation model that offers very good approximate estimation of layer thicknesses. These layer thickness estimations enable one to control the parameters for the coating process before starting experimental procedures. Furthermore, they are particularly important in fields of application where a precise amount of coating material on foam supports is highly desired. Using the combined techniques of dip coating and centrifugation, it is possible to apply tailor-made amounts of coating material on foam and to predict whether the cell size of the foam structure will remain open-celled after coating or not.

Pressure drop behavior of catalytic-coated foams is a very important characteristic for process engineering and hence plays a significant role in reactor design. For this reason, pressure drop measurements were carried out on SSiC foam samples with a geometry of 40 × 40 × 25 mm^3 and a cell size of 20 ppi at a velocity range of up to 15 m/s.

TABLE VI. Calculated layer thickness for dip coating step $d_{\mathrm{dip,si}}$ and spin coating step $d_{\mathrm{spin,si.}}$ depending on the sc of the coating slurry and rotational speed (N) of the centrifuge.

sc (wt%)	N (min^{-1})	$d_{\mathrm{dip,si.}} = d_{\mathrm{max.}}$ (µm)	$d_{\mathrm{spin,si.}}$ (µm)
	300		(63) → 35
45.4	400	35	35
	500		23
	300		(89) → 63
50.0	400	63	50
	500		32
	300		(138) → 83
53.7	400	83	78
	500		50

The pressure drop measurements were also performed after each single coating step of the multilayer system shown in Fig. 3 [uncoated foam (1) + rough particle layer (2) + mullite layer (3) + three various CA layer thicknesses (4a–c)] to demonstrate the influence of the layer thickness on the pressure drop. The permeability measurements of the uncoated and coated foams are represented in Fig. 8.

The pressure drop curves show a parabolic increase depending on the superficial air velocity (Fig. 8), which is a typical trend of open-celled foams. The increase in layer thickness that in turn decreases the cell diameter leads to an increase of pressure drop in an exponential manner. This relation can be described by the Hagen–Poiseuille law which states that the pressure drop inversely raises to the fourth power of the cell diameter.[60] The results obtained were analyzed according to the following Darcy–Forchheimer equation:

$$\frac{\Delta p}{D} = \frac{\eta}{k} v + \beta \rho v^2 \quad . \qquad (11)$$

where D is the thickness of the foam sample (25 mm), v is the superficial air velocity, η is the dynamic viscosity, ρ is the density of the flowing gas, k is the specific permeability, and β is the inertial coefficient.

Table IX shows the measured values of specific permeabilities, k, and inertial coefficients, β.

https://doi.org/10.1557/jmr.2013.127 Published online by Cambridge University Press

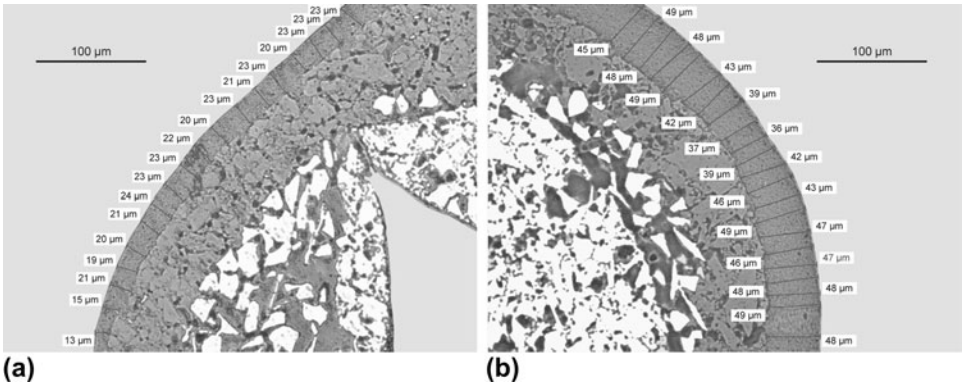


FIG. 5. Measurement of layer thickness on light microscopic images of perpendicular cut foam struts: (a) sc: 45 wt%; *N*: 400 m^{-1} and (b) sc: 50 wt%; *N*: 400 m^{-1}.

As expected, the specific permeability value decreases, whereas the inertial coefficient increases with increasing layer thickness values. Consequently, both the layer thickness and the homogeneity greatly influence the pressure drop behavior. This example demonstrates the importance of a well-defined coating on the resulting application characteristics.

TABLE VII. Measured layer thicknesses $d_{CA,Si.}$ depending on the sc and rotational speed *N*.

sc (wt%)	*N* (min^{-1})	$d_{CA,si.}$ (µm)
	300	38 ± 10.1
45.4	400	35 ± 6.4
	500	25 ± 4.8
	300	65 ± 5.1
50.0	400	50 ± 5.3
	500	31 ± 4.0
	300	78 ± 7.2
53.7	400	74 ± 4.9
	500	52 ± 8.5

IV. EXAMPLES AND APPLICATIONS

A. Rough surface layers

The purpose of a layer consisting of coarse particles is to improve the adhesion of secondary coatings or other materials such as composites. To develop these rough surfaces, a slurry of coarse particles has to be prepared and deposited on the foam struts by the previously described coating technique. This principle can be adapted to a large number of various ceramic and metallic foams.[61]

Figure 9 illustrates SSiC foam coated with rough SiC particles that could be used as a preform for MMCs (see Sec. IV. D).

As shown in Table X, the roughness of the resulting layer can be adjusted by the particle size of the applied powder. It can be seen that surface roughness increases with coarser particles, but specific surface area either remains or drops with highly coarse particles.

B. Catalytic coatings

An overview on scientific research with coated foams in catalysis was presented in Sec. III. A. In this section, the multilayered washcoat system, presented in Sec. III. D, is described in detail. As mentioned in the previous section, the CA washcoat provides a high specific surface area even at high temperatures of up to 1200 °C. Thus, the material combination is suitable for highly exothermic oxidation reactions where local overheating could occur. To use the developed material system in catalytic reactors, the CA washcoat was additionally impregnated with catalytically active component by using an ethanolic solution of manganese(II) nitrate tetrahydrate, which was then oxidized to form manganese oxide. Catalyst-coated foams made up of such a material combination were successfully tested in catalytic reactors for catalytic combustion of lean gases (<25% methane) obtained from landfills and coal mines.[62] They were also applied for the oxidation of CO in the afterburner of a solid oxide fuel cell system.[63]

Another possible practical application of catalytic-coated foams is the after treatment of exhaust in automobiles[64] or for the removal of soot from diesel exhaust gas.[65,66] In this field of application, honeycomb structures are mainly used due to their favorable pressure drop behavior and their resilience to vibrations.[67] Because of their ductility, metallic foams are also suitable materials for exhaust after treatment in automobiles. A comparison between catalytic-coated iron–chromium–aluminium (FeCrAl) alloy metallic foams and cordierite honeycombs has resulted in a promising catalytic activity. For these tests, metallic foams were coated with a mixed oxide washcoat containing ceria, ZrO_2, γ-Al_2O_3 and small amounts of precious metals (Fig. 10).

Another example within the context of catalysis is the catalytic combustion of waste gases from industrial processes. For this application, ceramic foams made of silicon carbide were coated with thin layers of a special perovskite-typed catalyst. Due to the open-celled structure and the

https://doi.org/10.1557/jmr.2013.127 Published online by Cambridge University Press

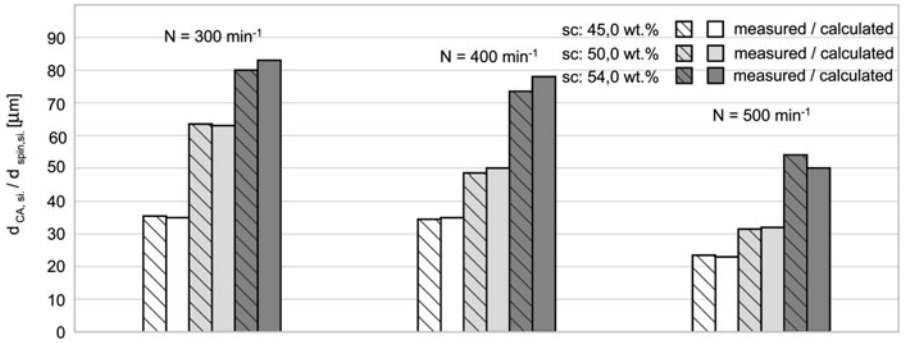
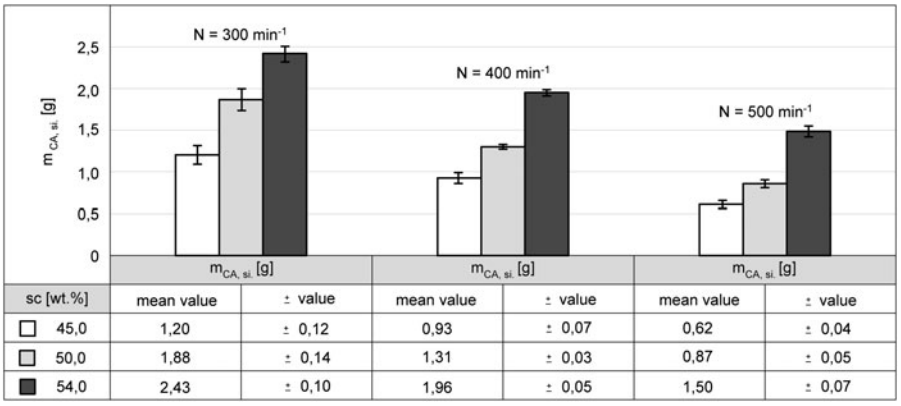


FIG. 6. Comparison of measured coating thicknesses $d_{CA,si.}$ and calculated values $d_{spin,si.}$.



	$m_{CA,si.}$ [g]		$m_{CA,si.}$ [g]		$m_{CA,si.}$ [g]	
sc [wt.%]	mean value	± value	mean value	± value	mean value	± value
45,0	1,20	± 0,12	0,93	± 0,07	0,62	± 0,04
50,0	1,88	± 0,14	1,31	± 0,03	0,87	± 0,05
54,0	2,43	± 0,10	1,96	± 0,05	1,50	± 0,07

FIG. 7. Measured mass ($m_{CA,si.}$) of sintered CA layers depending on the sc of the coating slurry and rotational speed N of the centrifuge.

low-density value of the foams, those material combinations can be heated by conventional external heating as well as by microwave radiation. Combining different ceramic substrates and coatings makes it possible to vary the heating behavior by microwaves. The combination of SSiC foam with perovskite catalyst coating shows excellent results in a pilot unit to clean air from high levels of vinyl acetate and methane at comparably low temperatures. The results are encouraging as this could save process energy and precious metal catalysts in industrial waste gas combustion.[68]

C. Adsorbent coatings

Another interesting field of application is the adsorption process utilized for the purification of exhaust gases, removal of hydrogen sulfide, or solvent recovery. In general, the industry, using fixed-bed reactors filled with activated carbon pellets or zeolite pellets. The main disadvantage of these fixed bed reactor structures is their high pressure drop. Another disadvantage is the occurrence of hot spots due to local overheating especially during the usage of activated carbon pellets. However, both drawbacks can be avoided by using coated foam structures instead. Figure 11 illustrates the possibility of homogeneous adsorbent coatings on cordierite foams without blocking the open-celled structure.

TABLE VIII. Comparison of calculated (d_{dw}) and measured ($d_{CA,Si.}$) layer thicknesses.

sc (wt%)	N (U/min)	ρ_s (G/cm^3)	$m_{CA,Si.}$ (G)	d_{dw} (µm)	$d_{CA,Si.}$ (µm)
45	400	0.75	0.93	33.7	34.5
	500		0.62	22.5	23.5
50	400	0.77	1.31	47.5	48.5
	500		0.87	31.5	31.5
54	400	0.78	1.96	71.0	73.5
	500		1.50	54.4	54.0

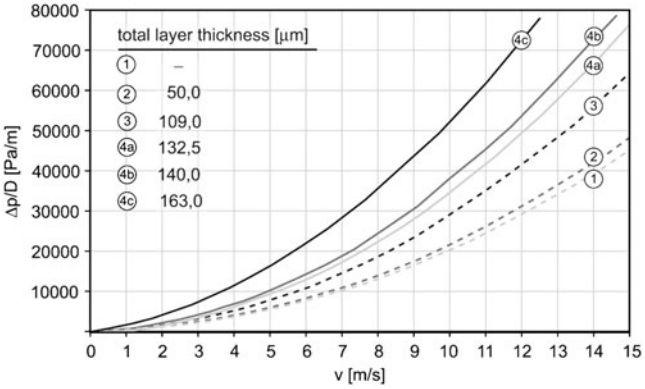


FIG. 8. Measured normalized pressure drop $\Delta p/D$ for an SSiC foam (20 ppi) as a function of superficial air velocity v for different total layer thicknesses [uncoated foam (1) + rough particle layer (2) + mullite layer (3) + three different CA layer thicknesses (Figs. 4a, 4b, and 4c)].

https://doi.org/10.1557/jmr.2013.127 Published online by Cambridge University Press

TABLE IX. Mean value and standard deviation of specific permeabilities k and inertial coefficients β of uncoated and step-by-step coated SSiC foams.

Layer		Coating thickness (μm)			
No.	Material	Single layer	All layers, summed up	Specific permeability k ($10^{-8} \times m^2$)	Inertial coefficient β (1/m)
1	Uncoated foam	...	...	17.9 ± 1.2	175 ± 5
2	Rough SSiC	50.0	50.0	14.3 ± 1.4	181 ± 10
3	Mullite	59.0	109.0	9.6 ± 0.8	242 ± 14
4(a)	CA	23.5	132.5	7.9 ± 0.4	291 ± 14
4(b)	CA	31.5	140.0	6.7 ± 0.5	310 ± 27
4(c)	CA	54.0	163.0	5.1 ± 0.6	356 ± 32

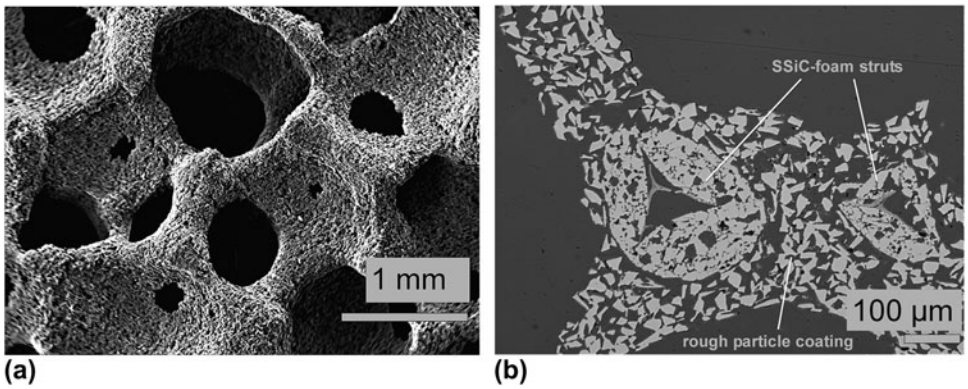


FIG. 9. Images of an SSiC foam with a rough surface layer: (a) SEM picture of foam topography and (b) cross-section of coated foam struts.

D. Preforms for MMCs

Over the last decades, ceramic foams as reinforcing preforms in MMCs have proven themselves since they offer cost-effective production methods in various attractive geometries.[69] Their main field of application is in wear protection and in increasing stiffness of light metals.[70] The foams are filled with metal using gravity and high-pressure casting techniques. One major problem is the dissimilar thermal expansion coefficient of metal and ceramics. This leads to delamination effects at the interface [Fig. 12(a)]. As a result, lower strength and Young's moduli were measured compared with the original metal properties. To overcome this mismatch and to form an interlocking mechanism between the metal and the ceramic, coating of coarse particles on the ceramic foam was applied. Preforms made of ceramic foams coated with rough surfaces were successfully applied using high-pressure die casting method. The metal infiltrated nearly all pores in the ceramic preform [Fig. 12(b)]. As a result, no delamination areas were observed and the measurements showed a high-specific stiffness of up to E/ρ = 42 GPa cm^3/g compared with the conventional Al or Mg alloys (E/ρ = 25–27 GPa cm^3/g).[71]

The tests were mainly conducted using foams with an ecd of 1000 μm. But it is also applicable for finer foams with ecds of 500 μm. One additional advantage of the functionalized coating is the higher ceramic content of the preform. Typical foam preforms with 10–15 wt% ceramic content show only limited improvements of wear protection and stiffness. With the described technique, however, ceramic contents of up to 30 wt% could be achieved resulting in better mechanical properties.

TABLE X. Roughness and specific surface area of SSiC foams coated with different particle sizes in comparison to a typical original SSiC foam surface; ecd 2.3 mm.

Sample	Surface roughness Rz (μm)	Specific surface area cm^2/cm^3
Original SSiC foam	10.1 ± 2.0	8330
SSiC coated with 23 μm particles	19.2 ± 1.7	8560
SSiC coated with 44 μm particles	42.9 ± 4.3	7350

E. Corrosion protection

There are several reasons for the application of corrosion protection layers to ceramic or metal foams. One often discussed subject is the degradation of foam materials in burner atmospheres, particularly of nonoxide ceramics or metals by oxidation.[72–74] Oxidation protecting layers could

https://doi.org/10.1557/jmr.2013.127 Published online by Cambridge University Press

enhance the lifetime of such components since they prevent the decrease of mechanical properties under such harsh conditions. Furthermore, protection layers are also useful against aggressive melts and chemicals. And third, intermediate layers are necessary to prevent reactions between coating and substrate, e.g., a mullite layer between CA coating and SiC substrate, as described in Sec. III. D. Following are the requirements to oxidation protection layers: their principal oxidation resistance, no reactions between layer and substrate at high temperatures, an excellent bonding as well as nearly similar coefficients of thermal expansion. For the variety of materials, the foam strut microstructure is mainly porous and hence show inner oxidation. Therefore, it is necessary to create coatings with dense microstructures compared with the struts. The following paragraph describes oxidation protection barrier coatings at SiC foams for burner applications.

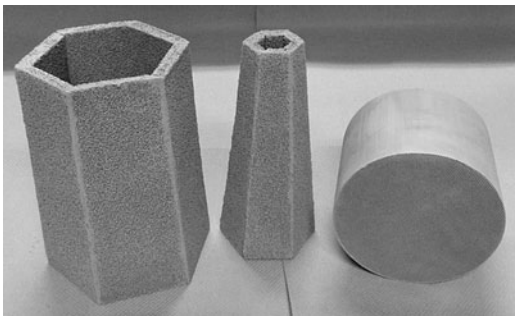


FIG. 10. FeCrAl foams (left and center) and cordierite honeycomb coated with a mixed oxide washcoat.

One concept consists of applying a mixture of alumina, yttria, and silicon carbide powders to generate a liquid yttrium–aluminium-garnet-phase during sintering to form a dense layer on the strut surface. The powders are coated by a multistage process (up to three steps) to seal cracks which occur during the sintering. The level of the oxidation protection was evaluated by measuring the mass

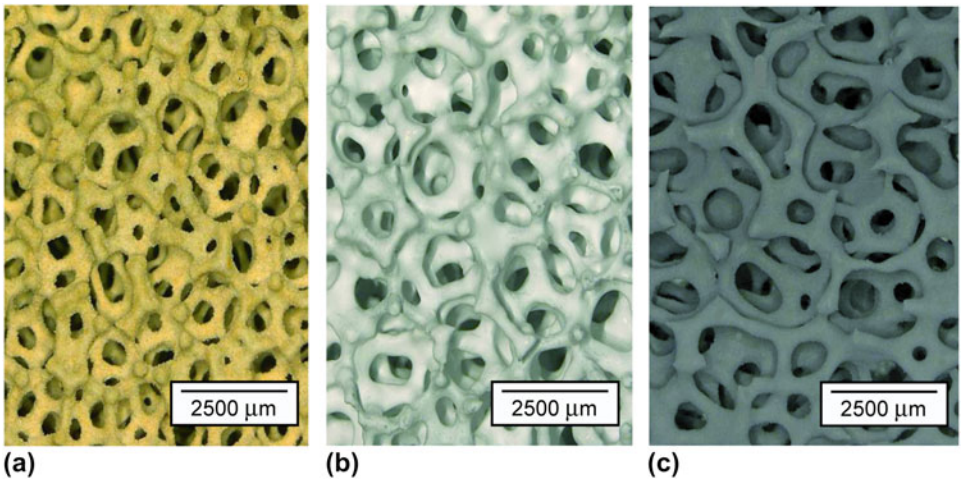


FIG. 11. Stereomicroscopic images of uncoated and adsorbent-coated cordierite foams for environmental engineering applications (a) uncoated cordierite foam, (b) zeolite coated, and (c) activated carbon coated.

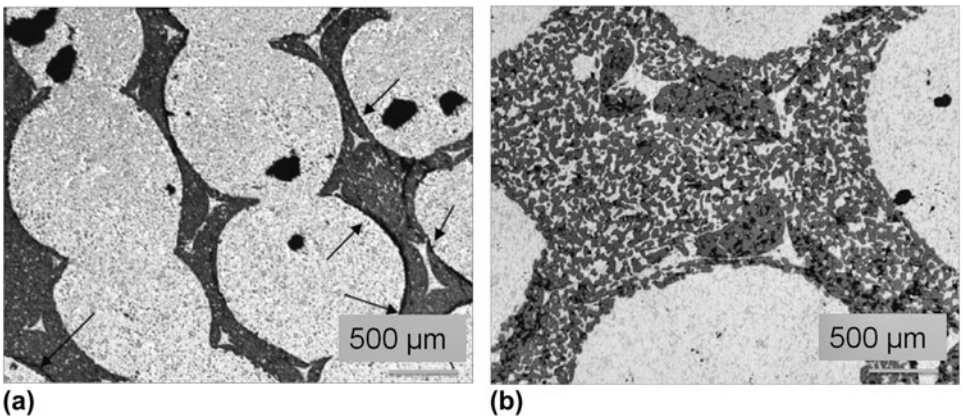


FIG. 12. (a) Micrographs of Al-infiltrated SSiC foams; bright: Al alloy, dark: SSiC. (a) Uncoated SSiC foam showing delaminations at the metal–ceramic interface (see arrows) and (b) SSiC foam coated with coarse particles after metal infiltration. No delamination is visible here.

https://doi.org/10.1557/jmr.2013.127 Published online by Cambridge University Press

change and electrical resistance after annealing at 1200 °C. It was discovered that, with increasing layer thickness, the mass change decreases and the electrical resistance is stabilized at about 1 MΩ at temperatures between 700 °C and 1000 °C.[75]

Another material concept for antioxidation coatings on open-celled SiC foams is the application of thin and strongly bonded mullite layers formed by slurries that consist of silicone resin and nano-sized alumina.[76]

V. CONCLUSIONS

In this paper, a two-stepped slurry-based technique of dip coating and centrifugation using a vertical centrifuge was developed for coating open-celled foams. The result indicates that homogeneous functional layers with a definite thickness of up to 100 μm could be deposited using shear-thinning slurries with high sc. The coating technology was applied and demonstrated by a complex multilayer system consisting of a thermal shock resistant SSiC foam as support, a layer with rough SiC particles, a mullite intermediate layer, and a CA washcoat.

A calculation model was derived to predict the coating thickness on foam struts based on the technological parameters of the developed coating technology and the shear-thinning flow behavior of the slurries. The model was successfully proved using the example of a CA washcoat layer. New process-relevant parameters have been identified to be used in the calculation model: first, the representative shear stress t_{rep} that significantly affects the formation of the layer thickness during centrifugation. And second, the minimal radial acceleration a_{r_min} that must be set as a minimum at the centrifuge to remove slurry from the saturated foam network ensuring homogenous and open-celled coatings. Consequently, the calculation model allows both quantitative estimation of the layer thickness and qualitative assessment of the resulting coating quality. Thus, the coating process can be precisely regulated.

In conclusion, a targeted application of the described coating technology in combination with the calculation model enables the production of tailor-made material combinations of "foam + functional layer." These offer a large number of practical applications in the field of process engineering and environmental technologies. This fact is illustrated by different material combinations such as layers made of coarse particles, zeolites, activated carbon, γ-Al_2O_3, perovskites, mullite, and yttria–alumina–garnet on SiC–, Al_2O_3–, or cordierite foams. These functionalized foams can be applied for a large number of applications, e.g., as adsorbents and catalysts at environmental engineering, as preforms for MMCs and for special purposes, which requires corrosion and oxidation resistance.

ACKNOWLEDGMENT

Parts of the presented work were financially supported by German Federal Ministry of Education and Research (BMBF) and BMWI (Grant Nos. 01LS05016 and AiF161ZBR/2).

NOMENCLATURE

a_r
radial acceleration
a_{r_min}
minimal radial acceleration
$d_{CA,si.}$
measured layer thicknesses of CA-washcoat
d_{dip}
layer thickness that is formed by dipping
d_{spin}
layer thickness that is formed by centrifugation (spinning)
$\bar{d}_{spin}$
medium layer thickness that is formed by centrifugation (spinning)
d_s
diameter of the foam strut
d_w
diameter of the cell window
D
foam thickness
E/ρ
specific stiffness
G'
storage modulus
G''
loss modulus
k
specific permeability
N
rotational speed of the centrifuge
Δp
pressure drop
sc
solid content
S_{geo}
specific geometrical surface area
s_{total}
drying and sinter shrinkage
V
superficial air velocity
Greek letters
β
inertial coefficient
ε_0
open foam porosity
η
dynamic viscosity

https://doi.org/10.1557/jmr.2013.127 Published online by Cambridge University Press

ρ
gas density
ρ_S
slurry density
τ_0
yield point
τ_{rep}
representative shear stress

REFERENCES

1. J. Adler and G. Standke: Offenzellige Schaumkeramik, Part 1/2, Keram. Z. 55(9/10), 694–703/786–792 (2003). [in German].
2. K. Schwartzwalder and A.V. Somers: Method of making porous ceramic articles. U.S. Patent No. 3090094, 1963.
3. D. Fino, N. Russo, G. Saracco, and V. Specchia: Multifunctional filter for treatment of the flue gases from municipal waste incinerators. *Ind. Eng. Chem. Res.* **44**, 9542–9548 (2005).
4. L. Giani, C. Cristiani, G. Groppi, and E. Tronconi: Washcoating method for Pd/[gamma]-Al_2O_3 deposition on metallic foams. *Appl. Catal., B* **62**, 121–131 (2006).
5. B.A.A. Van Setten, J. Bremmer, S.J. Jelles, M. Makkee, and J.A. Moulijn: Ceramic foam as a potential molten salt oxidation catalyst support in the removal of soot from diesel exhaust gas. *Catal. Today* **53**, 613–621 (1999).
6. K.C. Taylor: Ceramic foam filtration: No longer a band-aid. *Mod. Cast.* **94**, 25–28 (2004).
7. Anonym author: Clean metal, the 'Holy Grail' for all foundries. *Foundry J.* **180**, 283–285 (2006).
8. Anonym author: Ceramic foam. *J. Interceram.* **38**, 36 (1989).
9. K. Zhang and J. Zhu: Filtration technology - an effective way to improve quality of heavy iron castings. In *69th World Foundry Congress, Proceedings, Hangzhou, CN, Oct 16–20, 2010*.
10. M. Aslanowicz, L. Oscilowski, S. Pysz, J. Stachanczyk, and P. Wieliczko: Application of the ceramic filters in the gating systems for cast steel. *Przeglad Odlewnictwa* **55**, 652–659 (2005).
11. C.G. Aneziris, S. Dudczig, M. Emmel, H. Berek, G. Schmidt, and J. Hubalkova: Reactive filters for steel melt filtration. *Adv. Eng. Mater.* **15**, 46–59 (2013).
12. *Cellular Ceramics: Structure, Manufacturing, Properties and Applications*, edited by M. Scheffler and P. Colombo (Wiley-VCH: Weinheim, Germany, 2005).
13. E.C. Bucharsky, K.G. Schell, R. Oberacker, and M.J. Hoffmann: Preparation of transparent glass sponges via replica method using high-purity silica. *J. Am. Soc.* **93**, 111–141 (2010).
14. J. Adler and G. Standke: Open-celled silicon carbide foams made by replication method – manufacturing, properties and application of SSiC and SiSiC foams. In *Proceedings Intern. Conf. on porous ceramic materials, PCM 2005, 20–21 October at the Oud Sint-Jan, Bruges, CD-ROM, Flemish Institute for Technological Research*, 2005. 6 pages.
15. A. Ortona, S. Gianella, and D. Gaia: SiC foams for high temperature applications. In *Advances in Bioceramics and Porous Ceramics IV: Ceramic Engineering and Science Proceedings*, Vol. **32**, John Wiley & Sons, Inc., 2011; pp. 153–161.
16. J. Adler, G. Standke, M. Jahn, and F. Marschallek: Cellular ceramics made of silicon carbide ceramics for burner technology. *Ceram. Eng. Sci. Proc.* **29**, 271–286 (2009).
17. V. Paserin, S. Marcuson, J. Shu, and D.S. Wilkinson: CVD technique for Inco nickel foam production. *Adv. Eng. Mater.* **6**, 454–459 (2004).
18. J. Adler, K. Kümmel, P. Quadbeck, G. Standke, and G. Stephani: Synthesis of open-celled metal foams by replication technique. In: *Proceedings of the International Symposium on Cellular Metals for Structural and Functional Applications, CELLMET 2005*; B. Kieback and G. Stephani, ed., Fraunhofer IRB Stuttgart, 2005; pp. 199–205.
19. L.D. Zardiackas, D.E. Parsell, L.D. Dillon, D.W. Mitchell, L.A. Nunnery, and R. Poggie: Structure, metallurgy, and mechanical properties of a porous tantalum foam. *J. Biomed. Mater. Res. Part B* **58**, 180–187 (2001).
20. H.J. Ronold, S.P. Lyngstadaas, and J.E. Ellingsen: Analysing the optimal value for titanium implant roughness in bone attachment using a tensile test. *Biomaterials* **24**, 4559–4564 (2003).
21. A.D. Jatkar: *A New Catalyst Support Structure for Automotive Catalytic Converters*. SAE 971032, 1997.
22. G.C. Koltsakis, D.K. Katsaounis, I.A. Markomanolakis, Z.C. Samaras, D. Naumann, S. Saberi, and A. Böhm: *Metal Foam Substrate for DOC and DPF Applications*. SAE 2007-01-0659, 2007.
23. J. Adler, and G. Standke: Open-celled silicon carbide foam and method for production thereof. WO 02/20426 (2002).
24. J. Adler, A. Fuessel, D. Boettge, F. Marschallek, M. Jahn, and A. Michaelis: Cellular ceramics in combustion environments. In *Proceedings of the International Conference on Cellular Materials, CellMat 2010*; C. Stephani, T. Hipke, M. Scheffler, and J. Adler, eds., Deutsche Gesellschaft für Materialkunde e.V. DGM, Oberursel, 2010; pp. 137–142.
25. J. Adler, M. Teichgraeber, G. Standke, H. Jaunich, H. Stoever, and R. Stoetzel: Open-cell expanded ceramic with a high level of strength, and process for the production thereof. U.S. Patent No. 6 635 339 1997.
26. J. Adler and G. Standke: Si-sic LigaFill® foams and related net-like structures – new lightweight and low-cost materials for spaceborne applications, in *Materials for Transportation Technology*, Vol. **1**, edited by P.J. Winkler (Wiley-VCH Verlag GmbH & Co. KGaA, Weinheim, 2000), pp. 270–275. doi: 10.1002/3527606025.ch42.
27. P. Quadbeck, K. Kuemmel, R. Hauser, G. Standke, J. Adler, G. Stephani, and B. Kieback: Structural and material design of open-cell powder metallurgical foams. *Adv. Eng. Mater.*, Special Issue: Cellular Materials **13**, 1024–1030 (2011).
28. G. Standke, P. Quadbeck, K. Kümmel, H. Balzer, and A. Wierhake: Transfer of manufacturing process for stainless-steel foam to industrial scale. In *Cellular Materials Proceedings, CELLMAT 2012, Conventus Congressmanagement & Marketing GmbH Jena*, ISBN 978-3-00-039965-7 (2012).
29. R. Hauser, G. Standke, J. Heineck, G. Stephani, and P. Quadbeck: Open cell titanium foams for bone replacement. In *Proceedings of the International Conference on Cellular Materials, CellMat 2010*; G. Stephani, T. Hipke, M. Scheffler, and J. Adler, eds, Deutsche Gesellschaft für Materialkunde e.V. DGM, Oberursel, 2010; p. 61.
30. P. Quadbeck, K. Kuemmel, G. Stephani, G. Standke, J. Adler, and H. Uhlenhut: Molybdenum foams for heat insulation in industrial furnaces. In *Cellular Metals for Structural and Functional Applications, CELLMET 2008: Proceedings of the International Symposium on Cellular Metals for Structural and Functional Applications*; G. Stephani, ed., Fraunhofer IFAM, Dresden, 2009; p. 107–112.
31. J. Adler, G. Standke, D. Kopejzny, G. Stephani, K. Kuemmel, and W. Beckert: Thermal radiation shield for vacuum and protective atmosphere. U.S. Patent No. 2008/0131684 (2008).
32. R. Phelan, D. Weaire, and K. Brakke: Computation of equilibrium foam structures using the surface evolver. *Exp. Math.* **4**, 181–192 (1995).
33. *Standard Test Method for Cell Size of Rigid Cellular Plastics ASTM D 3576-77* (2004).
34. *PORE!SCAN product information*. http://www.giib.de/de/pore_scan.html, 2013.
35. L.J. Gibson and M.F. Ashby: *Cellular Solids: Structure and Properties*, 2nd ed. (Cambridge University Press, 1999), p. 16–38.
36. J.T. Richardson, Y. Peng, and D. Remue: Properties of ceramic foam catalyst supports: Pressure drop. *Appl. Catal., A* **204**, 19–32 (2000).

https://doi.org/10.1557/jmr.2013.127 Published online by Cambridge University Press

37. F.C. Buciuman and B. Kraushaar-Czarnetzki: Ceramic foam monoliths as catalyst carriers. 1. Adjustment and description of the morphology. *Ind. Eng. Chem. Res.* **42**, 1863–1869 (2003).
38. J. Grosse, B. Dietrich, G.I. Garrido, P. Habisreuther, N. Zarzalis, H. Martin, M. Kind, and B. Kraushaar-Czarnetzki: Morphological characterization of ceramic sponges for applications in chemical engineering. *Ind. Eng. Chem. Res.* **48**, 10395–10401 (2009).
39. L. Giani, G. Groppi, and E. Tronconi: Mass-transfer characterization of metallic foams as supports for structured catalysts. *Ind. Eng. Chem. Res.* **44**, 4993–5002 (2005).
40. A. Inayat, H. Freund, T. Zeiser, and W. Schwieger: Determining the specific surface area of ceramic foams: The tetrakaidecahedra model revisited *Chem. Eng. Sci.* **66**, 1179–1188, (2011).
41. R.J. Farrauto, Y. Liu, W. Ruettinger, O. Ilinich, L. Shore, and T. Giroux: Precious metal catalysts supported on ceramic and metal monolithic structures for the hydrogen economy. *Catal. Rev. Sci. Eng.* **49**, 141–196, (2007).
42. M. Haruta, Y. Souma, and H. Sano: Catalytic combustion of hydrogen-II. An experimental investigation of fundamental conditions for burner design. *Int. J. Hydrogen Energy* **7**, 729–736 (1982).
43. P. Chin, X. Sun, G.W. Roberts, and J.J. Spivey: Preferential oxidation of carbon monoxide with iron-promoted platinum catalysts supported on metal foams. *Appl. Catal., A* **302**, 22–31 (2006).
44. I. Cerri, G. Saracco, and V. Specchia: Methane combustion over low-emission catalytic foam burners. *Catal. Today* **60**, 21–32 (2000).
45. K. Jirátová, L. Morávková, J. Malecha, and B. Koutský: Ceramic foam in catalytic combustion of methane. *Collect. Czech. Chem. Commun.* **60**, 473–481 (1995).
46. A.N. Pestryakov, V.V. Lunin, A.N. Devochkin, L.A. Petrov, N.E. Bogdanchikova, and V.P. Petranovskii: Selective oxidation of alcohols over foam-metal catalysts. *Appl. Catal., A* **227**, 125–130 (2002).
47. Y. Wang, D.P. Vanderwiel, A.L.Y. Tonkovich, Y. Gao, and E.G. Baker: Catalyst structure and method of Fischer-Tropsch synthesis. U.S. Patent No. 2002099103 (2002).
48. R. Güttel, U. Kunz, and T. Turek: Reaktoren für die Fischer-Tropsch-Synthese. *Chemie Ingenieur Technik* **79**, 531–543 (2007) [in German].
49. A. Reitzmann, F.C. Patcas, and B. Kraushaar-Czarnetzki: Keramische Schwämme: Anwendungspotenzial monolithischer Netzstrukturen als katalytische Packungen. *Chemie Ingenieur Technik* **78**, 885–898 (2006) [in German].
50. J.T. Richardson and M.V. Twigg: Ceramic Foam Catalyst Supports Preparation and Properties. *MRS Proceedings*, **368**, 315 (1994).
51. M.V. Twigg and J.T. Richardson: Theory and applications of ceramic foam catalysts. *Chem. Eng. Res. Des.* **80**, 183–189 (2002).
52. M.V. Twigg and J.T. Richardson: Fundamentals and applications of structured ceramic foam catalysts. *Ind. Eng. Chem. Res.* **46**, 4166–4177 (2007).
53. B.A.A. Van Setten, C. van Gulijk, M. Makkee, and J.A. Moulijn: Molten salts are promising catalysts. How to apply in practice? *Top. Catal.* **16/17**, 275–278 (2001).
54. J.T. Richardson, M. Garrait, and J.K. Hung: Carbon dioxide reforming with Rh and Pt-Re catalysts dispersed on ceramic foam supports. *Appl. Catal., A* **255**, 69–82 (2003).
55. F.C. Buciuman and B. Kraushaar-Czarnetzki: Preparation and characterization of ceramic foam supported nanocrystalline zeolite catalysts. *Catal. Today* **69**, 337–342 (2001).
56. L. Landau and B. Levich: Dragging of a liquid by a moving plate. *Acta Phys. Chim. U.R.S.S.* **17**, 42–45 (1942).
57. A.G. Emslie, F.T. Bonner, and L.G. Peck: Flow of a viscous liquid on a rotating disk. *J. Appl. Phys.* **29**, 858–862 (1958).
58. T.G. Mezger: *Das Rheologie Handbuch 2. Auflage* (Vincentz Network GmbH & Co. KG, Hannover, 2006) [in German].
59. D. Boettge, J. Adler, and G. Standke: Cellular material for high-temperature applications and method for the production thereof. U.S. Patent No. WO2010/066649 (2010).
60. A.P. Philipse and H.L. Schram: Non-darcian airflow through ceramic foams. *J. Am. Ceram. Soc.* **74**, 728–732 (1991).
61. G. Standke, J. Adler, and D. Boettge: Open-cell ceramic and/or metal foams having a rough enveloping surface and a method for the production thereof. U.S. Patent No. WO2010/066648 (2010).
62. D. Boettge and J. Adler: Functionalization of ceramic foams for high-temperature catalytic applications illustrated by the development of a lean gas reactor. In *Proceedings of the International Conference on Cellular Materials, CellMat 2010*; G. Stephani, T. Hipke, M. Scheffler, and J. Adler, eds., Deutsche Gesellschaft für Materialkunde e.V. DGM, Oberursel, 2010; pp. 191–196.
63. M. Jahn, M. Heddrich, A. Weder, E. Reichelt, and R. Lange: Oxidative dry-reforming of biogas: Reactor design and sofc system integration. *Energy Technol.* **1**, 48–58 (2013).
64. A.N. Pestryakov, E.N. Yurchenko, and A.E. Feofilov: Foam-metal catalysts for purification of waste gases and neutralization of automotive emissions. *Catal. Today* **29**, 67–70 (1996).
65. B.A.A.L. Van Setten, J. Bremmer, S.J. Jelles, M. Makkee, and J.A. Moulijn: Ceramic foam as a potential molten salt oxidation catalyst support in the removal of soot from diesel exhaust gas. *Catal. Today* **53**, 613–621 (1999).
66. B.A.A.L. Van Setten, C. van Gulijk, M. Makkee, and J.A. Moulijn: Molten salts are promising catalysts. How to apply in practice? *Top. Catal.* **16/17**, 275–278 (2001).
67. W.M. Carty and P.W. Lednor: Monolithic ceramics and heterogeneous catalysts: Honeycombs and foams. *Curr. Opin. Solid State Mater. Sci.* **1**, 88–95 (1996).
68. D. Boettge, J. Adler, G. Standke, T. Krech, R. Krippendorf, and P. Scholz: Catalytically functionalized ceramic foams for exhaust gas treatment. In *Cellular Materials Proceedings, CELLMAT 2012, Conventus Congressmanagement & Marketing GmbH Jena*, ISBN 978-3-00-039965-7 (2012).
69. T. Zeuner, P. Stojanov, P. Busse, and P.R. Sahm: *7th European Conference on Composite Materials ECCM-7, London, May 14-16, 1996.* (Woodhead Publishing Ltd., Abington Hall, Cambridge, UK, 1996).
70. J. Schreiner, D. Regener, E. Ambos, and M. Ziesemann: *Konstruieren und Gießen* (4), 32 (2007).
71. G. Standke, T. Müller, A. Neubrand, J. Weise, and M. Göpfert: Cost-efficient metal-ceramic composites - novel foam-preforms, casting processes and characterisation. *Adv. Eng. Mater.* **12**, 189–196 (2010).
72. W. Acchar, E. Ramalho, F. Souza, W. Torquato, V. Rodrigues, and M. Innocentini: Characterization of cellular ceramics for high-temperature applications. *J. Mater. Sci.* **43**, 6556–6561 (2008).
73. A. Ortona, S. Pusterla, P. Fino, F.R.A. Mach, A. Delgado, and S. Biamino: Aging of reticulated SiSiC foams in porous burners. *Adv. Appl. Ceram.* **109**, 246–251 (2010).
74. M. Presas, J. Pastor, J. Lorca, A. Martín, J. Segurado, and C. González: Strength and toughness of cellular SiC at elevated temperature. Special issue honouring Professor Manuel Elices on the occasion of his 70th birthday, *Eng. Fail. Anal.* **16**, 2598–2603 (2009).
75. H.P. Martin, G. Standke, and J. Adler: A new oxidation protection strategy for silicon carbide foams. *Adv. Eng. Mater.* **10**, 227–234 (2008).
76. E. Bernardo, G. Parcianello, P. Colombo, J. Adler, and D. Boettge: Mullite monoliths, coatings and composites from a preceramic polymer containing alumina nano-sized particles, in *Advances in Polymer Derived Ceramics and Composites* (John Wiley & Sons, Inc., 2010), pp. 51–60.

https://doi.org/10.1557/jmr.2013.127 Published online by Cambridge University Press